

ANTIMICROBIAL AND OSTEOCONDUCTIVE PROPERTIES OF TWO DIFFERENT TYPES OF TITANIUM SILVER COATING

M.G. Kontakis^{1,*}, A. Diez-Escudero¹, H. Hariri², B. Andersson¹, J.D. Järhult³ and N.P. Hailer¹

¹ OrthoLab, Department of Surgical Sciences/Orthopaedics, Uppsala University, SE-751 85 Uppsala, Sweden

² Department of Medical Biochemistry and Microbiology, Uppsala University, Box 582, SE-751 23 Uppsala, Sweden

³ Department of Medical Sciences, Uppsala University, SE-751 85 Uppsala, Sweden

Abstract

In prosthetic joint surgery, Ag coating of implant areas in direct contact with bone has been met with hesitation for fear of compromising osseointegration. The physicochemical, antibacterial and osteoconductive properties of three different Ti samples were studied: Ti6Al4V alloy that was grit-blasted (GB), Ti6Al4V alloy with an experimental Ti-Ag-nitride layer (SN) applied by physical vapour deposition (PVD) and commercially available PVD-coated Ti6Al4V alloy with a base Ag layer and a surface Ti-Ag-nitride layer (SSN, clinically known as PorAg[®]). Ag content on the surface of experimental SN and SSN discs was 27.7 %wt and 68.5 % wt, respectively. At 28 d, Ag release was 4 ppm from SN and 26.9 ppm from SSN substrates. Colonisation of discs by *Staphylococcus aureus* was the highest on GB [$944 (\pm 91) \times 10^4$ CFU/mL], distinctly lower on experimental SN discs [$414 (\pm 117) \times 10^4$ CFU/mL] and the lowest on SSN discs [$307 (\pm 126) \times 10^4$ CFU/mL]. Primary human osteoblasts were abundant 28 d after seeding on GB discs but their adhesion and differentiation, measured by alkaline-phosphatase production, was suppressed by 73 % on SN and by 96 % on SSN discs, in comparison to GB discs. Thus, the PVD-applied Ag coatings differed considerably in their antibacterial effects and osteoconductivity. The experimental SN coating had similar antibacterial effects to the commercially available SSN coating while providing slightly improved osteoconductivity. Balancing the Ag content of Ti implants will be vital for future developments of implants designed for cementless fixation into bone.

Keywords: Silver, titanium, osteoconductivity, arthroplasty, periprosthetic joint infection, human osteoblasts, material analysis.

***Address for correspondence:** M.G. Kontakis, OrthoLab, Department of Surgical Sciences/Orthopaedics, Uppsala University, SE-751 85 Uppsala, Sweden.
Email: mikael.kontakis@gmail.com

Copyright policy: This article is distributed in accordance with Creative Commons Attribution Licence (<http://creativecommons.org/licenses/by-sa/4.0/>).

List of Abbreviations

ALP	alkaline phosphatase	LDH	lactate dehydrogenase
ANOVA	analysis of variance	MRSA	methicillin-resistant <i>Staphylococcus aureus</i>
ATCC	American Type Culture Collection	OB	osteoblast
AU	arbitrary units	PBS	phosphate-buffered saline
CFU	colony-forming unit	PI	propidium iodide
CVD	chemical vapor deposition	PJI	periprosthetic joint infection
DAPI	4',6-diamidino-2-phenylindole	PVD	physical vapour deposition
EDX	energy dispersive X-ray	R _a	arithmetical mean height of a line
FBS	foetal bovine serum	<i>S. aureus</i>	<i>Staphylococcus aureus</i>
GB	grit-blasted	S _a	arithmetical mean height of a surface
hOB	human osteoblast	SEM	scanning electron microscopy
ICP-OES	inductively coupled plasma optical emission spectroscopy	SN	Ti-Ag-nitride layer
		SSN	double layer consisting of a base Ag layer and a superficial SN
		TSB	tryptic soy broth

XRD	X-ray diffraction
α -MEM	minimum essential medium Eagle alpha modification

Introduction

A key step in the pathogenesis of a PJI on implants is bacterial adherence and formation of biofilm. Ag coating of different metallic devices implanted into the human body is a common strategy for preventing the early stages of the biofilm formation process (Klasen, 2000; Spriano *et al.*, 2018). In the context of orthopaedic surgery, these coatings should ideally fulfil the dual requirements of being both antimicrobial and osteoconductive, since their use is intended to inhibit bacterial proliferation without substantially interfering with the viability of surrounding bone tissue or with implant osseointegration (Albrektsson and Johansson, 2001; Hoover *et al.*, 2017).

Ti alloys, foremost Ti6Al4V, are commonly used in prosthetic joint surgery (Wang and Khoo, 2013). Several Ag-coated Ti implants are in clinical use, such as the galvanically Ag-coated MUTARS® (Implantcast) tumour prostheses, the PorAg® (Waldemar Link) coating applied on MegaC® (Waldemar Link) hip or knee megaprotheses by PVD and the Agluna® (Accentus Medical) coating of Stanmore tumour prostheses that carries the least amount of Ag (Fiore *et al.*, 2020). Such implants seem to reduce the risk of a PJI but conclusions are mainly based on retrospective, uncontrolled cohort studies with limited sample sizes (Wyatt *et al.*, 2019). In a recent observational study comparing Ag-coated and non-Ag-coated MUTARS® prostheses of the proximal femur, PJI rates were 9.4 % in patients treated with Ag-coated and 14.3 % in patients with uncoated implants (Streitbuerger *et al.*, 2019). In a similarly designed study on the same implant, the incidence of a PJI was 8.9 % after use of Ag-coated megaprotheses of the proximal tibia, while it was 16.7 % among patients within the non-Ag-coated implants (Hardes *et al.*, 2017). The PorAg® coating also conferred a relatively low risk of developing a PJI; however, this was observed in a non-comparative, rather heterogenous study design (Scocianti *et al.*, 2016). A case-control study of 170 patients (Wafa *et al.*, 2015) reported a 2-fold increase in PJI cases in a group of patients with non-Ag-coated implants compared to those receiving Ag-coated Agluna® implants (22 % *vs.* 11 %). Except for asymptomatic local argyria, toxic side effects seem to be rare (Glehr *et al.*, 2013; Hardes *et al.*, 2007a; Hussmann *et al.*, 2013) and Ag coating of orthopaedic implants is, thus, deemed a reasonable approach to reduce the risk of developing a PJI (Hardes *et al.*, 2010; Romanò *et al.*, 2019). It has to be noted that all the above mentioned commercially available Ag coatings are only applied on parts of the implant that are not intended for direct bone contact.

For clinically used implants, there are a limited amount of data on mechanisms of action, amount

of Ag released into surrounding compartments and antimicrobial properties against clinically relevant bacterial strains (Politano *et al.*, 2013; Romanò *et al.*, 2015; Wyatt *et al.*, 2019). Most *in vitro* studies use laboratory strains from the ATCC, examples are MRSA (ATCC 43300 or EDCC 5247), *Staphylococcus epidermidis* (SE RP62A, ATCC 35983 and DSM 18857), *Pseudomonas aeruginosa* (PA 01 or ATCC 9027), *S. aureus* (ATCC 6538, 12600 or 29213), *Streptococcus sanguinis* (NCTC 10904) or *Escherichia coli* (NRBC3972) (Amin Yavari *et al.*, 2016; Ando *et al.*, 2010; Besinis *et al.*, 2017; Das *et al.*, 2008; Devlin-Mullin *et al.*, 2017; Funao *et al.*, 2016; Khalilpour *et al.*, 2010; Kose *et al.*, 2013; Trujillo *et al.*, 2012; Zhao *et al.*, 2011). These strains have been isolated from skin lesions, nasopharynx and wounds but not specifically from patients with orthopaedic infections, raising questions around the validity of these models in the context of PJI research.

There is relatively little information on how Ag-coated Ti surfaces interact with OBs, but this question is of high interest if uncemented fixation of Ag-coated Ti implants intended for direct bone contact were to be used. hOB adhesion to Ag-coated Ti surfaces would be crucial to achieve solid secondary stability in the host bone but most experimental studies on Ag-coated Ti have used OB-like cell lines but not hOBs (Spriano *et al.*, 2018).

The use of hOBs together with patient-specific bacterial strains would help the understanding of the clinical efficacy of Ag-coated Ti implants and unravel their interactions with cells and bacteria, but no such study has hitherto been performed (Devlin-Mullin *et al.*, 2017; Hardes *et al.*, 2007b; Spriano *et al.*, 2018). Thus, the present study explored the physicochemical and biological properties of two different Ag coatings of Ti, one commercially available (PorAg®) and one experimental, and compared them to a GB Ti alloy (PoroLink®). PorAg® is a relatively thick dual-layer Ag coating, but it is not present on parts of the implant that are intended for bone ingrowth. The experimental Ag coating that has not yet been in clinical use is thinner, as it lacks the base Ag layer, and has the objective of maintaining antimicrobial effects while potentially enabling cementless fixation in the host bone. To enhance the validity of the study models, a PJI-derived *S. aureus* strain was used to investigate the antimicrobial properties of these coatings, and adhesion and differentiation of primary hOBs on these samples were examined.

Materials and Methods

Three types of Ti6Al4V alloy-based discs, with a diameter of 12.5 mm and a thickness of 2 mm, were used for all experiments. The first group consisted of PoroLink®, GB Ti discs; the second group with the experimental coating, consisted of the same Ti6Al4V alloy, without grit-blasting, but instead featuring a monolayer of SN; the third group consisted of Ti6Al4V

alloy coated with the SSN coating, commercially known as PorAg[®] (patent number US8845751B2 endoprosthesis component, 2014-09-30). All disc groups consisted of the same Ti6Al4V substrate and the Ag coatings were created by PVD. The discs and their coatings were manufactured by Waldemar Link GmbH & Co KG (Hamburg, Germany). In the SSN discs, the underlying Ag layer had a thickness of ~ 1 µm, while the TiAgN on top was about 0.1 µm thick. According to the manufacturer, the molar fraction of Ag in the coatings was XAg = 10 % ± 2 % for SN and XAg = 20 % ± 4 % for SSN. All samples were sterilised by gamma irradiation prior to the experiments.

Material characterisation

Phase characterisation of the bulk samples was investigated by XRD using a D8 Advance diffractometer (Bruker) equipped with a Cu K α anode and Ni filter and operated at 40 kV and 40 mA. Data acquisition was performed in the range of 5–80° 2 θ with a step of 0.02° and 1 s per step. The experimental patterns obtained were compared to those of Ti (JCDPS 44-1294), corundum (JCDPS 01-085-1337), Ag (JCDPS 01-1164) and Ti nitride (JCDPS 38-1420). Surface morphology was investigated by SEM (Merlin, Zeiss) and chemical composition by EDX for each substrate. Measurements of surface roughness were carried out using white light interferometry (NexView ZYGO, Ametek Inc, Weiterstadt, Germany) on each sample (4 samples for each material), scanning a surface of 1.68 × 1.68 mm² at 4 different sites for each single sample. The average results were computed for both the profile average height (R_a) and the area profile average height (S_a).

Colonisation of discs with *S. aureus*

The discs were colonised with the *S. aureus* strain AN-1400743, which was isolated from a PJI patient previously treated at the University Hospital of Uppsala. For each experiment, the strain was thawed and incubated overnight on blood agar. Then, 1 µL of bacterial isolate, defined by the use of a 1 µL loop, was added to 4 mL of sterile 0.9 % wt NaCl solution (Sigma-Aldrich), further diluted by a factor of 50,000 in sterile 0.9 % wt NaCl solution and finally diluted another 10-fold in TSB, creating the bacterial suspension used for subsequent experiments. To calculate the number of bacteria present in this suspension, 100 µL aliquots of the suspension were incubated on blood agar for 24 h at 37 °C and the mean viable bacterial yield was 857 ± 298 CFU/mL.

The discs were placed in a 50 mL sterile centrifuge tube that contained 3 mL of the final bacterial suspension. As a control for each tested group, one disc was incubated with 3 mL of bacteria-free TSB. Discs were incubated at 37 °C (Termarks, B9130, Bergen, Norway) with the original bacterial suspension for 24 h, 72 h and 10 d to find the optimal incubation time. To remove non-adherent bacteria,

the discs were rinsed twice in 10 mL sterile 0.9 % NaCl solution.

Fluorescent assay for biofilm viability

The biofilm that had been formed after the incubation was stained using the LIVE/DEAD[™] Biofilm Viability Kit according to the manufacturer's instructions (LIVE/DEAD BacLight Bacterial Viability Kit, Thermo Fischer Scientific). Briefly, 150 µL of the nucleic acid staining solution (3 µL/mL SYTO[®]9 and 3 µL/mL PI) dissolved in distilled water was added onto the previously colonised Ti discs and incubated at room temperature for 30 min in the dark. The excess dye was aspirated, the sample gently rinsed with sterile saline solution and fluorescence was analysed by confocal laser scanning microscopy (Carl Zeiss LSM 700). SYTO[®]9 was excited at 488 nm and emission measured at 540 nm; PI was excited at 555 nm and emission measured at 590 nm. The intensity was set at 2 % of the laser power and the object was observed with a pinhole diameter of 1 AU. For each disc, three random positions were scanned and acquired images were processed using Fiji software (Web ref. 1).

Biofilm detachment assay and colony quantification

Enzymatic detachment was performed for the quantification of biofilm formation using *S. aureus*, as previously described by Doll *et al.* (2016). 4 mg/mL collagenase type I and 2 mg/mL dispase type II were dissolved in PBS and 600 µL were transferred to each well containing a single disc. The implant discs were left in the shaker at 37 °C and 220 rpm for 2 h. After incubation, the implants were vortexed for 2 min to completely detach adherent bacteria, the supernatant was serially diluted (10-fold, 100-fold, 1,000-fold and 10,000-fold) in sterile saline and aliquots of 100 µL were plated on blood agar. After incubation for 24 h at 37 °C, colonies were counted and the results were expressed as CFU/mL. To assess the efficacy of enzymatic detachment, an additional LIVE/DEAD[™] assay of the discs was performed as above mentioned after enzymatic detachment.

The presence of bacteria on the implant surface was assessed by SEM (Merlin, Zeiss, Germany) at an operating voltage of 3 kV and a working distance of 6 mm after 24, 48 and 72 h of incubation. The discs were rinsed in PBS and immersed for 30 min at room temperature in 2.5 % glutaraldehyde in PBS (Sigma-Aldrich). Afterwards, samples were rinsed with PBS and dehydrated through series of increasing ethanol concentrations (10, 30, 50, 70, 90 and 100 %). Finally, discs were coated with a 5 nm layer of Au/Pd and investigated by SEM.

hOB isolation and culture

All cells were isolated after approval by the Swedish Ethical Review Authority (approval number: 2020-04462). hOBs were isolated from femoral heads of 6 human donors undergoing hip replacement, as previously described (Helfrich and Ralston, 2012).

The finely diced bone fragments were placed in 25 cm² flasks containing α -MEM (GE Healthcare) supplemented with 10 % FBS (Sigma-Aldrich), 2 mmol/L L-glutamine, 50 U/mL penicillin and 50 μ g/mL streptomycin (SVA, Uppsala, Sweden). The medium was refreshed weekly until the cells were approximately 90 % confluent (4-6 weeks). 25 cm² flasks were used for passage 1 and 2, while from passage 3, cells were cultured in 75 cm² flasks. Passage 2 and 3 of hOBs were used for cell culture experiments.

Prior to seeding, the discs were incubated for 24 h at 37 °C and 5 % CO₂ in 24-well plates (1.9 cm²/well) in α -MEM supplemented with 10 % FBS and 1 % penicillin/streptomycin. The next day, cell medium was removed and 1 mL of the cell suspension containing 10⁵ cells was added onto the discs. Wells without discs were seeded similarly and used as internal controls. The seeded discs were incubated with cell medium for 7 d without medium exchange. After 7 d, the cell medium was replaced with osteoinduction medium based on the above cell medium but with the addition of β -glycerophosphate (10 mmol/L; Sigma-Aldrich), ascorbic acid (50 μ L/mL; Sigma-Aldrich) and dexamethasone (100 nmol/L; Sigma-Aldrich) and exchanged once every 7 d for the remaining 3 weeks, giving a total culture time of 4 weeks.

Assessment of hOB adhesion and differentiation

The seeded discs were transferred to new 24-well plates and washed with 1 mL PBS once, before adding 400 μ L lysis buffer (C2978, Sigma-Aldrich). Then, the multiwell plates were placed on a shaker for 15 min at room temperature and cell lysates were collected and used for further measurements. Cell adhesion was quantified by LDH reaction (TOX7, Sigma-Aldrich) according to manufacturer's specifications. To assess cell viability, intracellular LDH was measured from cell lysates. Briefly, 100 μ L of LDH solution were added to 50 μ L of cell lysate and incubated at 37 °C for 30 min, followed by absorbance measurement at 490 and 690 nm using a spectrophotometer (Tecan, Männedorf, Switzerland). Cell differentiation was investigated by ALP concentrations in cell lysates. Briefly, 100 μ L of ALP substrate (Sigma-Aldrich) was added to 50 μ L of cell lysate and incubated at 37 °C for 30 min before measuring absorbance at 405 nm wavelength. ALP and LDH values for each sample were normalised to the control values corresponding to cells cultured in the absence of discs.

Cellular cytoskeletons and nuclei were investigated using fluorescence microscopy after 4 weeks of culture. For phalloidin staining of the cytoskeleton, the seeded discs were transferred to a 24-well plate containing 1 mL PBS per well. Cells were fixed with 4 % buffered formaldehyde for 10 min. 100 μ g phalloidin (P1951, Sigma-Aldrich) were dissolved in 95 % ethanol to a concentration of 50 μ g/mL. The formaldehyde-fixed cells were permeabilised using

0.1 % Triton X-100 (USB Corporation, Cleveland, OH, USA) for 5 min and then 40 μ L of the phalloidin solution were added per well. The plates remained at room temperature for 40 min, then discs were rinsed twice with PBS and 1 mL of DAPI (Life Technologies) stain was added to each well. For discs where only DAPI staining was performed, cells were not permeabilised with Triton X-100. After 60 min incubation at room temperature in the dark, the DAPI solution was removed by aspiration and the discs were rinsed twice with PBS. The plates with the discs were immersed in PBS solution and stored at 4 °C until microscopy imaging was performed.

Image acquisition and analysis

The discs were analysed using a Leica inverted microscope (Leica DMi8, Microsystem CMS GmbH, Wetzlar, Germany) using Leica Application Suite X (LasX, Leica Microsystems) software. 5 images per disc were acquired using a 20 \times objective at a mean exposure of 18-20 ms and a gain of 10 AU. Focus depth correction was applied due to cell dispersion along the Z-axis. CellProfiler software (version 3.1.8, Broad Institute, Cambridge, MA, USA) was used to quantify cell numbers by counting the DAPI positive nuclei per image using an adapted pipeline. Briefly, cellular nuclei were identified after all non-elliptical shapes were eliminated and luminosity correction filters were applied. A global threshold was used for the identification of primary objects.

Ag release

The Ag ion release into the supernatant from GB, SN and SSN discs seeded with hOBs was quantified by ICP-OES (Avio 200, PerkinElmer) at specific time points (1, 2, 3, 5, 7, 9, 14, 19, 21, 26 and 28 d). The measurements were conducted under Ar plasma at a flow rate of 1 mL/min. Calibration was performed using dilutions of stock standard solutions (1 μ g/mL, 10 μ g/mL and 100 μ g/mL). The supernatants from 3 specimens ($n = 3$) of each sample type were collected at each time point and analysed by ICP-OES using dilutions into 2 % HNO₃. A blank containing cell medium both with and without cells was included as matrix standard. Data are presented as cumulative and non-cumulative Ag release for each investigated time point.

Statistics

Data distribution was described using mean, median, interquartile range and standard deviation. For comparisons of mean between groups, one-way ANOVA followed by pairwise *t*-test using the Benjamini-Hochberg method was carried out and the level of significance was set at $p < 0.05$. If the assumption of homogeneity of variances was violated, as determined by Levene's test, Welch's robust test was performed. R software version 3.6.1 (Web ref. 2) and the packages "readx1", "dplyr", "Hmisc", "car" and "Gmisc" were used.

Results

Material characterisation

Phase characterisation by XRD (Fig. 1a) showed typical α -Ti peaks for all substrates. GB discs showed peaks corresponding to Al oxide consistent with the grit-blasting process that is performed using corundum. The two Ag coatings differed in composition: the experimental SN discs showed peaks of Ti together with Ag and nitride, while SSN substrates depicted highly crystalline phases of Ti and Ag. The colour mapping of surface elemental contents investigated by EDX (Fig. 1c; green: Ti; blue: Ag; red: nitrogen) further evidenced the difference in compositions. GB contained Ti together with Al, V, O and C, whereas both Ag-coated Ti substrates contained mainly Ti, Ag and N. Ag constituted 27.7% of the total material mass on the surface of SN discs, amounting to less than half the amount of Ag measured on SSN discs that contained 68% of surface mass (Fig. 1b). SN featured Ag clusters whereas SSN showed a more homogenous distribution of Ag (Fig. 1c). Cumulative Ag release analysed by ICP was higher from SSN compared to SN discs (Fig. 1d). GB discs were also analysed, but no Ag release was detected (data not shown). After 4 d, the Ag release for both Ag-coated discs yielded approximately 3–6 ppm. After 5 d, SSN Ag release increased substantially, while SN reached

a steady release after 9 d of approximately 4 ppm. SSN discs' release increased along with the cell culture time, reaching values up to 26.9 ppm at 28 d.

The surface morphology, assessed by interferometry, indicated higher surface roughness of GB discs (Fig. 1b, 2b,d), compared to the Ag-coated discs (Fig. 2h,l), and larger surface grains (Fig. 2c,g,k). GB discs had a R_a of 12.5 μm and S_a of 14.41 μm . The microstructure of both Ag coatings varied substantially despite having similar surface roughness values. SN, with a surface roughness (R_a) of 1.75 μm exhibited heterogeneous pores (Fig. 2f) with small grains (Fig. 2g), while SSN with a surface roughness (R_a) of 1.79 μm had homogeneously distributed circular pores (Fig. 2j) and larger grains than SN (Fig. 2k).

Assessment of antimicrobial activity

After incubation of discs with planktonic (*i.e.* freely floating) *S. aureus*, bacteria adhered, became sessile and initiated the formation of a biofilm. On uncoated GB discs there was a noticeable increase in the area covered by biofilm after 72 h of incubation, followed by a less dynamic progression up to 10 d (Fig. 3a). The most noticeable difference between 72 h and 10 d was the number of dead bacteria, which was increased at 10 d. The CFU yields ($n = 2$) of implants incubated for 24 h were lower in comparison to 72 h and 10 d.

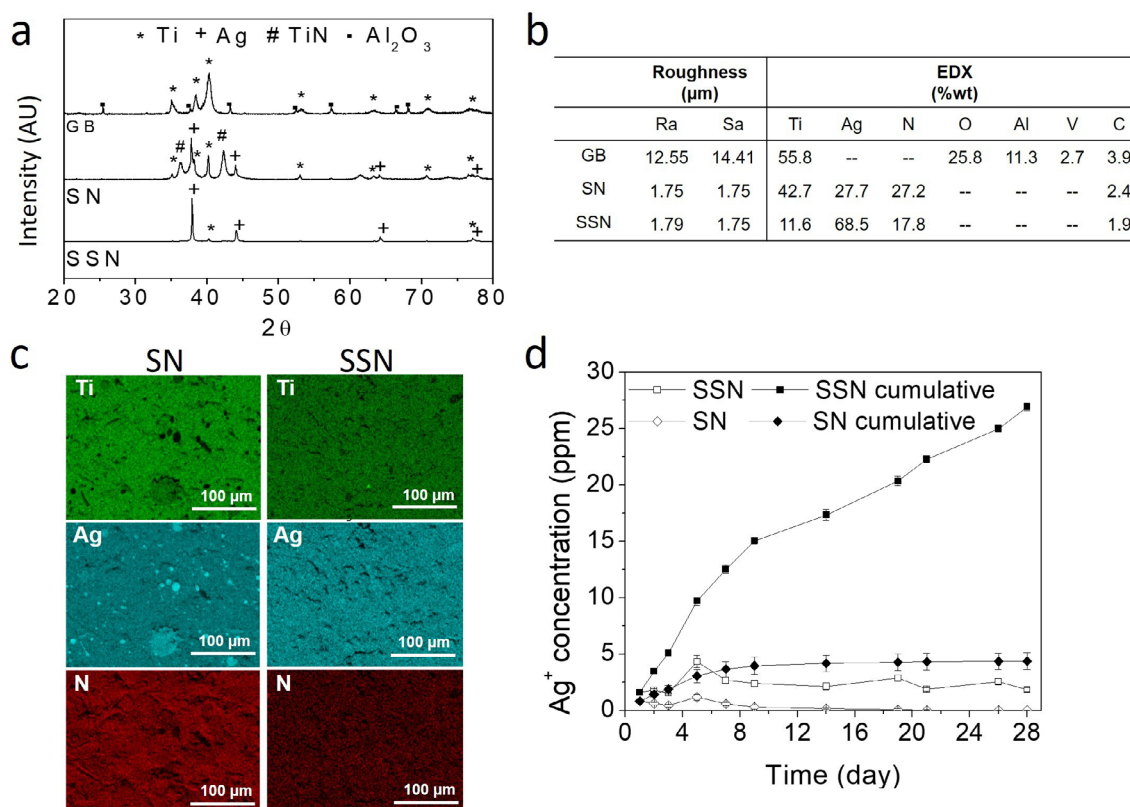


Fig. 1. Material characterisation of GB (PoroLink[®]), experimental SN coating and clinically used SSN (PorAg[®]). (a) XRD analysis of the surfaces showing crystalline phases. (b) Interferometry for surface roughness and quantitative % wt EDX results. (c) EDX colour mapping of the surface chemistry of experimental Ag-coated SN discs (left column) and commercially available SSN discs (right column). (d) Ag release as measured with ICP-OES ($n = 3$); hollow points are presenting the Ag release for each day; full points are presenting the cumulative release.

In addition, the differences between CFU yields after 72 h and 10 d were moderate (Fig. 3b). On GB discs, $1,017.5 \times 10^4$ CFU/mL ($\pm 140.7 \times 10^4$) were counted after 72 h, with a very modest and statistically non-significant increase to $1,097 \times 10^4$ CFU/mL ($\pm 89 \times 10^4$) after 10 d ($p = 0.61$). On SN discs, 398×10^4 CFU/mL ($\pm 21.2 \times 10^4$) were counted after 72 h, as compared to 506.5×10^4 CFU/mL ($\pm 43.1 \times 10^4$) after 10 d ($p = 0.18$). On SSN discs, 288.5×10^4 CFU/mL ($\pm 10.6 \times 10^4$) were counted after 72 h and 409.5×10^4 CFU/mL ($\pm 125.1 \times 10^4$) after 10 d ($p = 0.47$). For that reason, further microbiological assays were read out after 72 h, which were based on 7 biological replicates, each performed in triplicate.

The SEM images at 24 h, 48 h and 72 h evidenced a smaller amount of bacterial colonisation on SSN discs, with slightly more colonisation being present on SN, while GB displayed the largest amount of adherent bacteria (Fig. 4). In the LIVE/DEAD™ assay of different disc types after 72 h, it became apparent that SN and SSN discs were covered by biofilm to a lesser extent than the uncoated GB discs (Fig. 5a). The increased number of dead bacteria in GB could be explained by higher total bacterial counts being present on GB discs when compared to SN and SSN discs. *S. aureus* biofilm formation on GB was more homogenous whereas it was disrupted on SN and SSN discs. The number of dead bacteria (indicated by red fluorescence) was larger on SSN discs than on SN.

In the CFU yield assay following enzymatic detachment, the biofilm derived from GB discs after 72 h contained the largest number of CFU/mL (Fig. 5b). The mean CFU concentration derived from biofilm formed on GB discs was 944×10^4 ($\pm 91 \times 10^4$) CFU/mL, while the concentration in biofilm formed

on SN discs was 414×10^4 ($\pm 117 \times 10^4$) CFU/mL ($p < 0.01$). Biofilm formed on SSN discs gave rise to a mean 307×10^4 CFU/mL ($\pm 126 \times 10^4$), but the difference compared to the SN discs was not statistically significant ($p = 0.052$).

hOB adhesion and differentiation

hOBs visualised by DAPI/phalloidin staining 28 d after seeding showed very different densities and morphologies on the 3 investigated discs (Fig. 6). Cells on GB discs covered a larger area, producing a confluent monolayer, with round, prominent nuclei and typical cytoskeleton. On the SN discs, the cell layer was not always confluent and islands of cell aggregates with smaller, irregular nuclei were present in some areas. In SSN discs, the cells were sparse, had small nuclei and contracted cytoskeleton. They also had the tendency to form aggregates. Image analysis was used to quantify the observations above, supporting that GB discs were covered by a larger number of cells compared to SN and SSN (Fig. 6). The presented results were based on technical duplicates or triplicates, with a total of 3 biological replicates. On GB discs, a larger mean number of 149 ± 43 cells/image field was counted compared to 60 ± 55 cells/image field on SN discs; however, this difference was not statistically significant ($p = 0.057$). Cell numbers on SN discs were considerably larger than on SSN discs, where a mean of 4 ± 3.6 cells/image field was found, despite not being statistically significant ($p = 0.14$). However, the difference in cell numbers was statistically significant between GB and SSN ($p < 0.05$).

The following results were based on 4 biological replicates, with 2 to 5 technical replicates per biological replicate. LDH measurement from cell

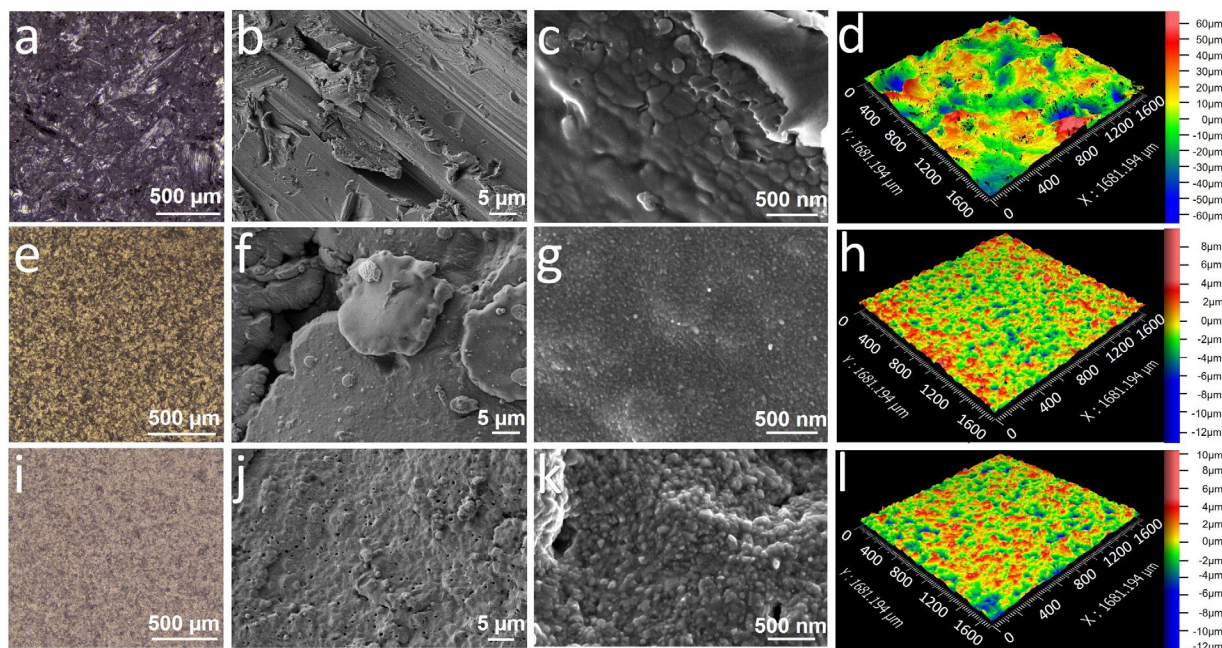


Fig. 2. Images of the different substrates obtained by SEM and 3D surface roughness maps obtained by interferometry. (a-d) Surface morphology of GB. (e-h) Surface morphology of SN. (i-l) Surface characteristics of SSN.

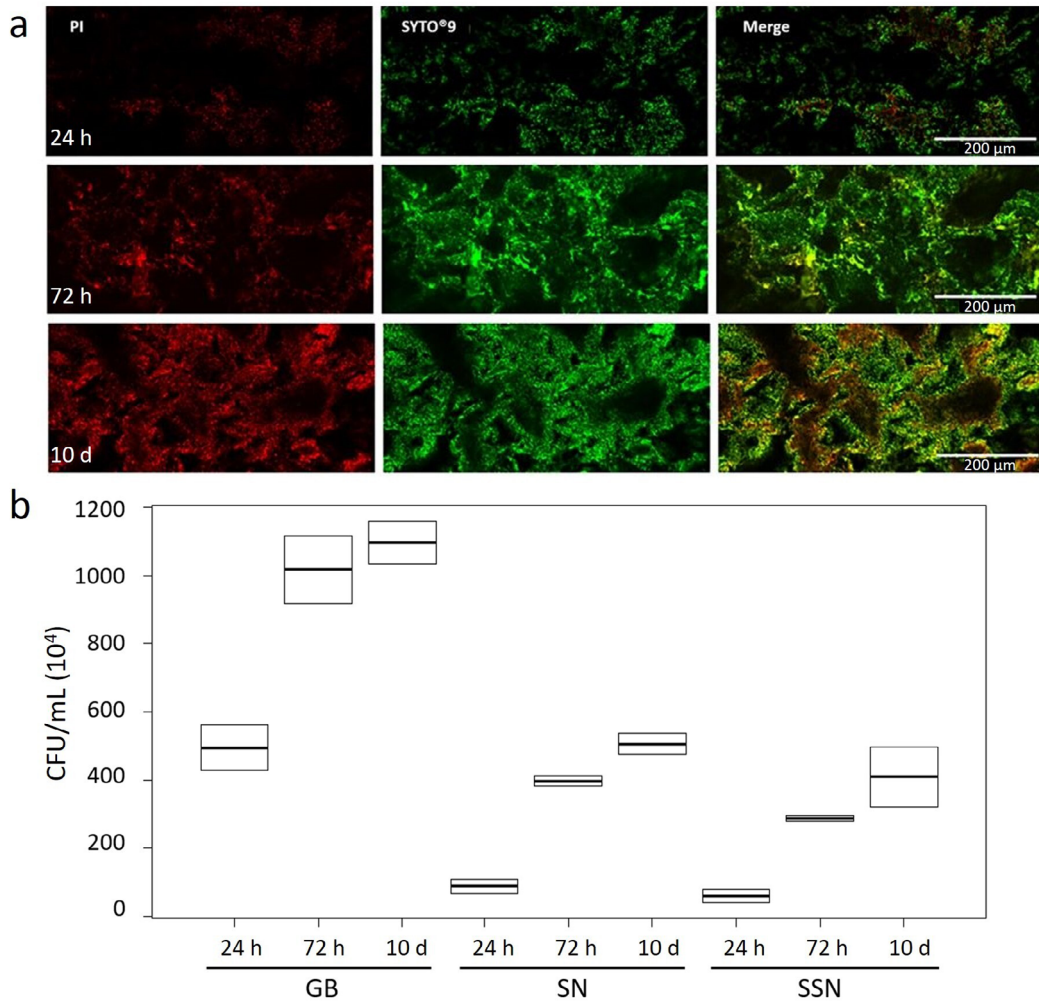


Fig. 3. Biofilm viability assays at different time points. (a) LIVE/DEAD™ confocal images of GB samples after different incubation periods with an *S. aureus* strain (red-propidium iodide: dead bacteria; green-SYTO⁹: live bacteria). Biofilm formation after 24 h, 72 h and 10 d. (b) Number of CFU/mL measured at different time points ($n = 2$) on the 3 investigated samples: GB, SN and SSN.

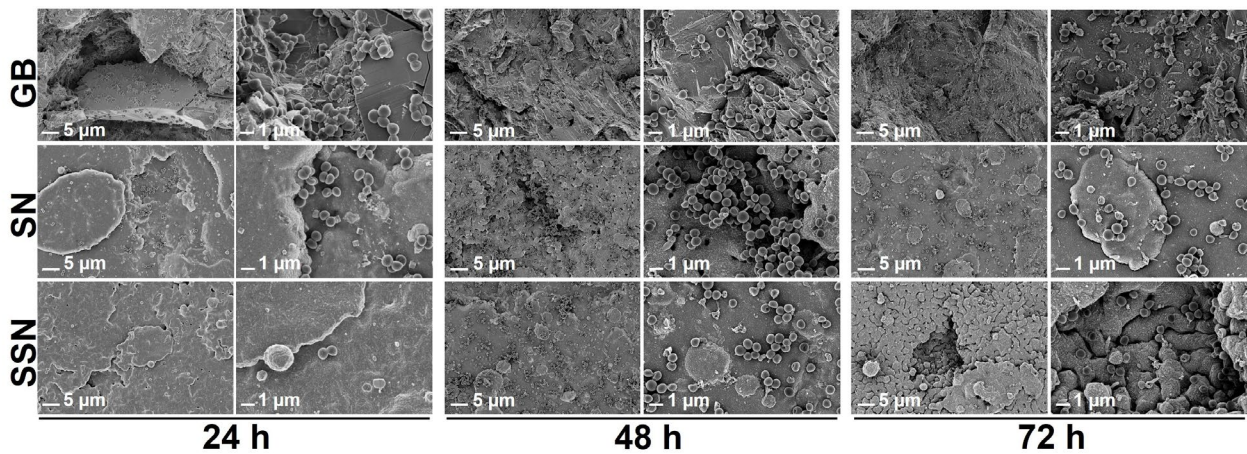


Fig. 4. SEM images of bacteria on GB, SN and SSN at different magnifications showing biofilm growth after 24, 48 and 72 h.

lysates (Fig. 7) was the highest after culture of hOBs on GB discs, with a mean of 1.08 ± 0.28 AU, compared to 0.49 ± 0.34 AU on SN ($p < 0.05$). LDH was the lowest in lysates from SSN discs, at 0.04 ± 0.04 AU, much lower than GB ($p < 0.01$). The difference in LDH measurement from hOB lysates that were cultured on SN or SSN was also statistically significant ($p < 0.05$). ALP release from cell lysates was the highest after culture of hOBs on GB discs, with a mean of 0.60 ± 0.35 AU, compared to 0.16 ± 0.19 AU from hOBs cultured on SN and 0.02 ± 0.01 AU from hOBs cultured on SSN (Fig. 7). The difference in ALP release between GB and SSN was statistically significant, as was the difference between GB and SN ($p < 0.05$). SN and SSN were not statistically different ($p = 0.41$).

Discussion

Due to the antibacterial properties of Ag coating of orthopaedic implants, some consider using it as a means to prevent and possibly treat a PJI. However, since Ag ions confer a multitude of cytotoxic effects,

adverse effects on the osteoconductive properties of Ag-coated Ti are a potential obstacle to the widespread use of this appealing method (Albers *et al.*, 2013). In the present study, two different Ag coatings of Ti alloys, one clinically used (SSN, PorAg[®]) and one experimental (SN), were investigated and compared to a GB Ti alloy without Ag coating.

Due to the grit-blasting process, GB discs had a higher surface roughness than the Ag-coated discs and analysis of the chemical surface composition of GB indicated the presence of alumina, reflecting the blasting procedure with corundum. The two investigated Ag coatings differed in composition and morphology, although they had a similar surface roughness. SSN discs had a considerably larger Ag content (more than double the amount) than the experimental SN counterparts, as illustrated by both XRD and EDX analysis. That could explain the larger Ag release from SSN surfaces, in comparison to SN.

Moderate surface roughness (R_a : 1-2 μm) has been demonstrated to promote osteoblast adhesion and osteogenesis (Feller *et al.*, 2015). On the other hand, higher surface roughness ($R_a > 0.2 \mu\text{m}$) correlates

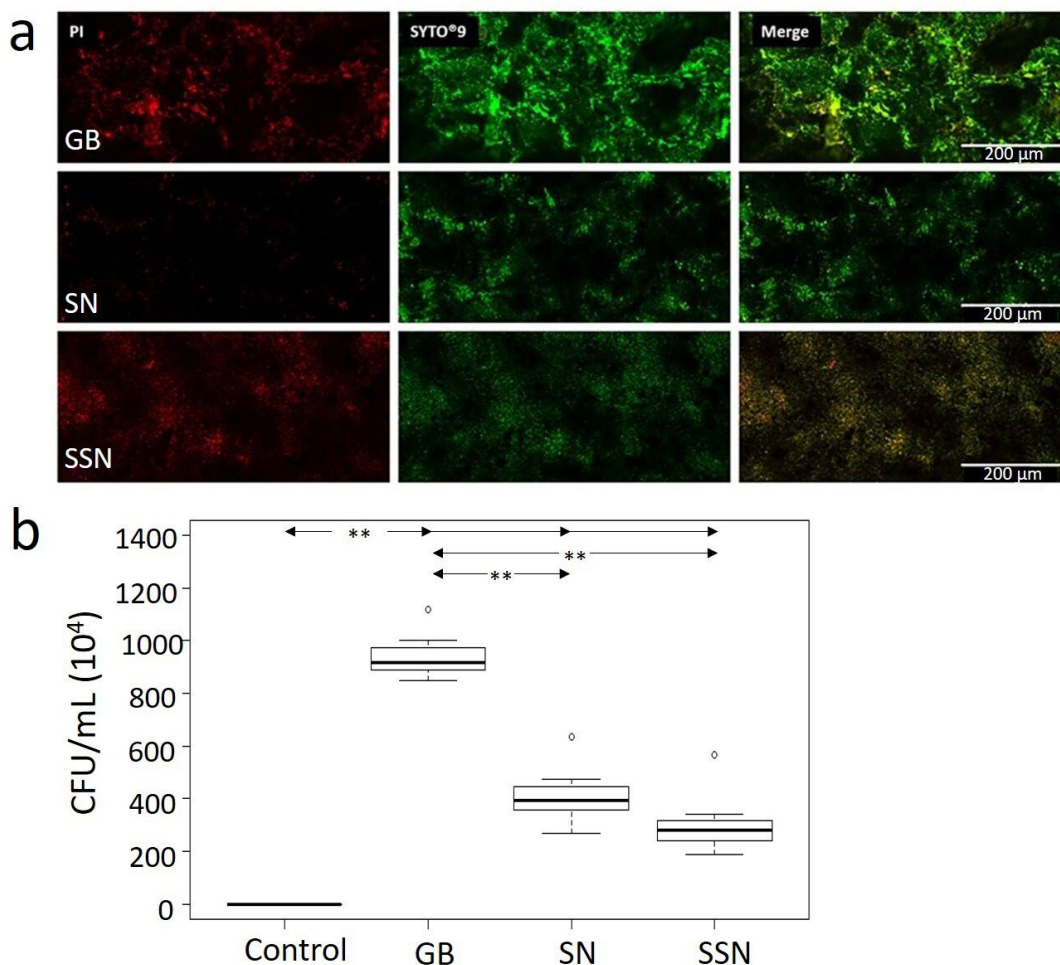


Fig. 5. Incubation of implant discs for 72 h, yield of colony forming units. (a) Dead bacteria in red (PI), live bacteria in green (SYTO[®]9). **(b)** CFU/mL count after 72 h of incubation on GB, SN and SSN discs ($n = 7$). The largest amount of biofilm was formed on GB discs as compared to the experimental SN coating and the commercial SSN. ** $p < 0.01$

with enhanced bacterial adhesion (Mas-Moruno *et al.*, 2019), which is in agreement with the larger number of CFUs/mL present in biofilm derived from GB discs. GB, with the highest surface roughness of all investigated discs, allowed the largest number of CFU to form, followed by SN and SSN. Similarly to previous studies (Albers *et al.*, 2013; Ewald *et al.*, 2006), the antimicrobial activity of the coatings increased with higher Ag content. Ag release investigated in the supernatants up to 4 weeks showed that SSN released up to 6 times more ionic Ag than experimental SN

coatings. Accordingly, the antimicrobial effect of SSN was stronger than that of SN, although the difference was not statistically significant. However, further studies are required to elucidate a dose-dependency between bactericidal effect and Ag-ion release.

To date, clinically available Ag coatings are mostly applied on parts of the implants that are not in direct contact with host bone (Harden *et al.*, 2007a; Harden *et al.*, 2017; Streitbueger *et al.*, 2019; Wafa *et al.*, 2015), with the singular exception of the Kyocera[®] coating of cementless cups and stems for

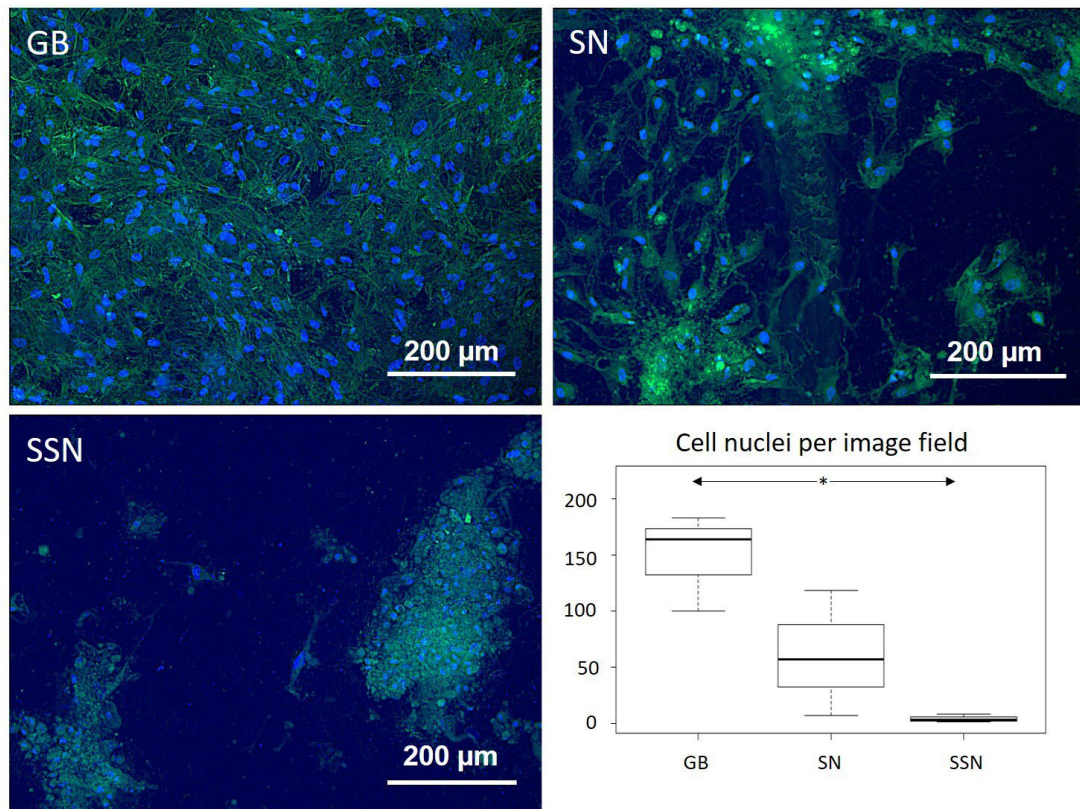


Fig. 6. hOBs on GB, SN and SSN stained with DAPI (blue) for nuclei and phalloidin (green) for cytoskeleton. Boxplots showing cellularity per image field after quantitative image analysis ($n = 3$). * $p < 0.05$.

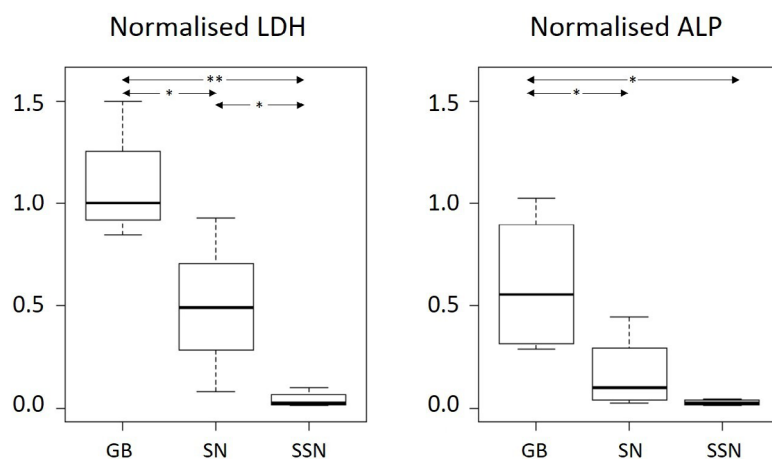


Fig. 7. Boxplot graphs of LDH and ALP production from the hOB lysates from GB, SN and SSN discs ($n = 4$). ** $p < 0.01$, * $p < 0.05$.

use in primary total hip arthroplasty that contains extremely small amounts of Ag (Eto *et al.*, 2015; Eto *et al.*, 2016; Kawano *et al.*, 2019). However, the presumed cytotoxic effects of Ag on OBs are of crucial importance if cementless fixation of Ag-coated Ti is considered. *In vivo* studies demonstrated that higher concentrations of Ag reduced bacterial colonisation of coated implants, however, with a concomitant negative impact on OB viability (Eto *et al.*, 2015; Liu and Man, 2017; Spriano *et al.*, 2018). This is supported by a study on Ti alloys sputtered with Ag that had antibacterial activity but lacked osteoconductivity (Wojcieszak *et al.*, 2017). Liu and Man (2017) investigated thicker Ag coatings containing up to 2 wt % Ag combined with hydroxyapatite on Ti alloys and found antibacterial activity against *S. aureus* with preserved osteoconductivity in a model using mice calvaria-derived bone cells. Prabu *et al.* (2015) found an Ag-dependent toxicity of Ag-coated Ti alloys using OB-like MG63 cells. With regard to Ag release, concentrations of Ag up to 5 ppm in simulated body fluid were found to be biocompatible while at the same time effective against *S. aureus*. In addition, a study on the effects of Ag nanoparticles in human mesenchymal stem cells showed a dose-dependent reduction in ALP, osteocalcin and osteoid production after osteoinduction (Sengstock *et al.*, 2014). In line with these results, larger amounts of Ag on the surface of the discs, as investigated in the present study, reduced the number of hOBs on the disc surface. Experimental SN discs, releasing smaller amounts of Ag than the SSN discs coated with the established PorAg[®] coating, induced a 67 % reduction in hOB numbers, while SSN reduced their numbers by 98 % when compared to the GB substrates. LDH measured in cell lysates reflected a cell viability reduction of 55 % in SN and 74 % in SSN when compared to the GB substrates. Similarly, ALP expression was reduced by 73 % in cell lysates from OBs that were seeded on SN and a 96 % reduction was observed on SSN when compared to the ALP expression of cells grown on GB. In addition to a decrease in cell numbers, cell shape seemed gravely affected on SSN discs, with OBs forming aggregates consisting of cells with small nuclei. These apoptotic hOB aggregates should not be confused with the bone-forming noduli that appear on rougher or hydroxyapatite-coated Ti surfaces (Eto *et al.*, 2015; Ewald *et al.*, 2006; Perizzolo *et al.*, 2001). Thus, SSN had a detrimental effect on cell viability, whereas SN retained a strong antibacterial effect causing at the same time less harm to hOBs.

Factors such as coating technique, layer thickness and implant surface modification are important in establishing a biofilm-inhibiting and at the same time osteoconductive interface. For instance, the canine model by Hauschild *et al.* (2015) constitutes an example of suppressed osseointegration of press-fit Ag-coated hip stems despite satisfactory roughness. The Ag coating was applied by PVD and it alternated with layers of a SiO_xCy polymer applied by CVD, as

a strategy to minimise the release of Ag over time and sustain cell viability.

Different coating techniques lead to different functionalities. In the experimental SN coating, Ag ions were integrated into the Ti and nitride layer, providing satisfactory antibacterial effects. Thus, adjusting the molecular fraction of Ag on Ti could lead to a reduced release of Ag ions that is more compatible with osteoblast survival and, thus, potentially applicable for cementless fixation. In contrast, the established coating with an intermediate Ag layer (SSN) underneath a superficial interrupted layer of AgTiN led to a prolonged and larger release of Ag ions with potentially negative effects on OBs. Therefore, SSN coatings are useful for parts of the implant that are not in contact with the bone.

Eto's group has explored the use of osteoconductive materials in combination with Ag (Eto *et al.*, 2015). They used flame spraying to coat Ti rods with a powder containing hydroxyapatite and Ag. Interestingly, rods that contained hydroxyapatite with 50 wt % Ag had much lower anchorage strength than rods containing hydroxyapatite alone 2 weeks after press-fit implantation into rat femora, but that difference was abolished after 4 and 6 weeks. The same group showed that primary total hip arthroplasty implants coated with hydroxyapatite containing 3 wt % Ag (KYOCERA[®], Kyocera Medical, Osaka, Japan) were both stable and infection-free, albeit in a small, non-comparative cohort (Eto *et al.*, 2016; Noda *et al.*, 2009). Bone ingrowth was histologically described on KYOCERA[®]-coated cups in 2 patients who had their implants revised for hip dislocation (Kawano *et al.*, 2019).

A strength of the present study was the use of primary hOBs derived from actual patients and not OB cell lines such as MG-63 or Saos-2, which each bears their own disadvantages (Czekanska *et al.*, 2012). Moreover, the use of an *S. aureus* strain that was isolated from an actual patient with a PJI added to the generalisability of the findings to a clinical setting. Additionally, 2 of the investigated coatings are today clinically used under the trade names PoroLink[®] (GB) and PorAg[®] (SSN), with PorAg[®] being applied on areas of megaprotheses that are not in contact with the host bone. Weaknesses of the study included the use of only one bacterial strain and the lack of *in vivo* data, including biomechanical testing of the anchorage strength of Ag-coated implants, but future experiments will address such issues.

Conclusions

Ag-coated Ti implants investigated in the present study conferred significant inhibitory effects on bacterial adhesion and biofilm formation, but they were considerably less osteoconductive than uncoated GB Ti. However, the experimental thinner Ag coating promoted hOB adhesion and differentiation better than the clinically used dual-layer Ag coating

(PorAg[®]), although their antibacterial properties were similar. Differences in Ag thickness, Ag release and the subtle differences in surface morphology of the two Ag substrates might be reasons underlying the improved osteoconduction on SN discs. These results supported the use of the already established coating with high Ag content (SSN) in patients at high risk of developing a PJI where osseointegration is not needed (*i.e.* cemented megaprotheses). Although the experimental Ag coating containing smaller amounts of Ag was slightly less toxic to OBs, further research on coatings with different porosities and Ag contents is needed before cementless fixation of Ag-coated implants can be explored under clinical conditions.

Acknowledgements

Authors would like to thank the Swedish Research Council (VR 2018-02612) for funding and Waldemar Link GmbH & Co KG (Hamburg, Germany) for kindly providing the discs used in the study.

NPH declares to have received institutional funding and lecturer's fees from Waldemar Link GmbH.

References

- Albers CE, Hofstetter W, Siebenrock KA, Landmann R, Klenke FM (2013) *In vitro* cytotoxicity of silver nanoparticles on osteoblasts and osteoclasts at antibacterial concentrations. *Nanotoxicology* **7**: 30-36.
- Albrektsson T, Johansson C (2001) Osteoinduction, osteoconduction and osseointegration. *Eur Spine J* **10**: S96-S101.
- Amin Yavari S, Loozen L, Paganelli FL, Bakhshandeh S, Lietaert K, Groot JA, Fluit AC, Boel CHE, Alblas J, Vogely HC, Weinans H, Zadpoor AA (2016) Antibacterial behavior of additively manufactured porous titanium with nanotubular surfaces releasing silver ions. *ACS Appl Mater Interfaces* **8**: 17080-17089.
- Ando Y, Miyamoto H, Noda I, Sakurai N, Akiyama T, Yonekura Y, Shimazaki T, Miyazaki M, Mawatari M, Hotokebuchi T (2010) Calcium phosphate coating containing silver shows high antibacterial activity and low cytotoxicity and inhibits bacterial adhesion. *Mater Sci Eng C* **30**: 175-180.
- Besinis A, Hadi SD, Le HR, Tredwin C, Handy RD (2017) Antibacterial activity and biofilm inhibition by surface modified titanium alloy medical implants following application of silver, titanium dioxide and hydroxyapatite nanocoatings. *Nanotoxicology* **11**: 327-338.
- Czekanska EM, Stoddart MJ, Richards RG, Hayes JS (2012) In search of an osteoblast cell model for *in vitro* research. *Eur Cells Mater* **24**: 1-17.
- Das K, Bose S, Bandyopadhyay A, Karandikar B, Gibbins BL (2008) Surface coatings for improvement of bone cell materials and antimicrobial activities of Ti implants. *J Biomed Mater Res B Appl Biomater* **87**: 455-460.
- Devlin-Mullin A, Todd NM, Golrokhi Z, Geng H, Konerding MA, Ternan NG, Hunt JA, Potter RJ, Sutcliffe C, Jones E, Lee PD, Mitchell CA (2017) Atomic layer deposition of a silver nanolayer on advanced titanium orthopedic implants inhibits bacterial colonization and supports vascularized *de novo* bone ingrowth. *Adv Healthc Mater* **6**: 1-14.
- Doll K, Jongstaphongpun KL, Stumpp NS, Winkel A, Stiesch M (2016) Quantifying implant-associated biofilms: comparison of microscopic, microbiologic and biochemical methods. *J Microbiol Methods* **130**: 61-68.
- Eto S, Kawano S, Someya S, Miyamoto H, Sonohata M, Mawatari M (2016) First clinical experience with thermal-sprayed silver oxide-containing hydroxyapatite coating implant. *J Arthroplasty* **31**: 1498-1503.
- Eto S, Miyamoto H, Shobuike T, Noda I, Akiyama T, Tsukamoto M, Ueno M, Someya S, Kawano S, Sonohata M, Mawatari M (2015) Silver oxide-containing hydroxyapatite coating supports osteoblast function and enhances implant anchorage strength in rat femur. *J Orthop Res* **33**: 1391-1397.
- Ewald A, Glückermann SK, Thull R, Gbureck U (2006) Antimicrobial titanium/silver PVD coatings on titanium. *Biomed Eng Online* **5**: 1-10.
- Feller L, Jadwat Y, Khacissa RAG, Meyerov R, Schechter I, Lemmer J (2015) Cellular responses evoked by different surface characteristics of intraosseous titanium implants. *Biomed Res Int* **2015**: 171945. DOI: 10.1155/2015/171945.
- Fiore M, Sambri A, Zucchini R, Giannini C, Donati DM, De Paolis M (2020) Silver-coated megaprosthesis in prevention and treatment of peri-prosthetic infections: a systematic review and meta-analysis about efficacy and toxicity in primary and revision surgery. *Eur J Orthop Surg Traumatol* **31**: 201-220.
- Funao H, Nagai S, Sasaki A, Hoshikawa T, Tsuji T, Okada Y, Koyasu S, Toyama Y, Nakamura M, Aizawa M, Matsumoto M, Ishii K (2016) A novel hydroxyapatite film coated with ionic silver *via* inositol hexaphosphate chelation prevents implant-associated infection. *Sci Rep* **6**: 2-10.
- Glehr M, Leithner A, Friesenbichler J, Goessler W, Avian A, Andreou D, Maurer-Ertl W, Windhager R, Tunn PU (2013) Argyria following the use of silver-coated megaprotheses: no association between the development of local argyria and elevated silver levels. *Bone Jt J* **95-B**: 988-992.
- Hardes J, Ahrens H, Gebert C, Streitbuenger A, Buerger H, Erren M, Gunsel A, Wedemeyer C, Saxler G, Winkelmann W, Gosheger G (2007a) Lack of toxicological side-effects in silver-coated megaprotheses in humans. *Biomaterials* **28**: 2869-2875.
- Hardes J, Von Eiff C, Streitbuenger A, Balke M, Budny T, Henrichs MP, Hauschild G, Ahrens H (2010) Reduction of periprosthetic infection with

silver-coated megaprotheses in patients with bone sarcoma. *J Surg Oncol* **101**: 389-395.

Hardes J, Henrichs MP, Hauschild G, Nottrott M, Guder W, Streitburger A (2017) Silver-coated megaprosthesis of the proximal tibia in patients with sarcoma. *J Arthroplasty* **32**: 2208-2213.

Hardes J, Streitburger A, Ahrens H, Nusselt T, Gebert C, Winkelmann W, Battmann A, Gosheger G (2007b) The influence of elementary silver *versus* titanium on osteoblasts behaviour *in vitro* using human osteosarcoma cell lines. *Sarcoma* **2007**: 1-5.

Hauschild G, Hardes J, Gosheger G, Stoeppeler S, Ahrens H, Blaske F, Wehe C, Karst U, Höll S (2015) Evaluation of osseous integration of PVD-silver-coated hip prostheses in a canine model. *Biomed Res Int* **2015**: 1-10.

Helfrich MH, Ralston SH (2012) *Bone Research Protocols*. Humana Press. DOI: 10.1007/978-1-61779-415-5.

Hoover S, Tarafder S, Bandyopadhyay A, Bose S (2017) Silver doped resorbable tricalcium phosphate scaffolds for bone graft applications. *Mater Sci Eng C* **79**: 763-769.

Hussmann B, Johann I, Kauther MD, Landgraber S, Jäger M, Lendemans S (2013) Measurement of the silver ion concentration in wound fluids after implantation of silver-coated megaprotheses: Correlation with the clinical outcome. *Biomed Res Int* **2013**: 1-11.

Kawano S, Sonohata M, Eto S, Kitajima M, Mawatari M (2019) Bone ongrowth of a cementless silver oxide-containing hydroxyapatite-coated antibacterial acetabular socket. *J Orthop Sci* **24**: 658-662.

Khalilpour P, Lampe K, Wagener M, Stigler B, Heiss C, Ullrich MS, Domann E, Schnettler R, Alt V (2010) Ag/SiOx/Cy plasma polymer coating for antimicrobial protection of fracture fixation devices. *J Biomed Mater Res Part B Appl Biomater* **94**: 196-202.

Klasen HJ (2000) A historical review of the use of silver in the treatment of burns. II. Renewed interest for silver. *Burns* **26**: 131-138.

Kose N, Otuzbir A, Pekşen C, Kiremitçi A, Doğan A (2013) A silver ion-doped calcium phosphate-based ceramic nanopowder-coated prosthesis increased infection resistance basic research. *Clin Orthop Relat Res* **471**: 2532-2539.

Liu X, Man HC (2017) Laser fabrication of Ag-HA nanocomposites on Ti6Al4V implant for enhancing bioactivity and antibacterial capability. *Mater Sci Eng C* **70**: 1-8.

Mas-Moruno C, Su B, Dalby MJ (2019) Multifunctional coatings and nanotopographies: toward cell instructive and antibacterial implants. *Adv Healthc Mater* **8**: e1801103. DOI:10.1002/adhm.201801103.

Noda I, Miyaji F, Ando Y, Miyamoto H, Shimazaki T, Yonekura Y, Miyazaki M, Mawatari M, Hotokebuchi T (2009) Development of novel thermal sprayed antibacterial coating and evaluation of release

properties of silver ions. *J Biomed Mater Res Part B Appl Biomater* **89**: 456-465.

Perizzolo D, Lacefield WR, Brunette DM (2001) Interaction between topography and coating in the formation of bone nodules in culture for hydroxyapatite- and titanium-coated micromachined surfaces. *J Biomed Mater Res* **56**: 494-503.

Politano AD, Campbell KT, Rosenberger LH, Sawyer RG (2013) Use of silver in the prevention and treatment of infections: silver review. *Surg Infect (Larchmt)* **14**: 8-20.

Prabu V, Karthick P, Rajendran A, Natarajan D, Kiran MS, Pattanayak DK (2015) Bioactive Ti alloy with hydrophilicity, antibacterial activity and cytocompatibility. *RSC Adv* **5**: 50767-50777.

Romanò CL, Tsuchiya H, Morelli I, Battaglia AG, Drago L (2019) Antibacterial coating of implants: are we missing something? *Bone Jt Res* **8**: 199-206.

Romanò CL, Scarponi S, Gallazzi E, Romanò D, Drago L (2015) Antibacterial coating of implants in orthopaedics and trauma: a classification proposal in an evolving panorama. *J Orthop Surg Res* **10**: 1-11.

Scoccianti G, Frenos F, Beltrami G, Campanacci DA, Capanna R, (2016) Levels of silver ions in body fluids and clinical results in silver-coated megaprotheses after tumour, trauma or failed arthroplasty. *Injury* **47**: S11-S16.

Sengstock C, Diendorf J, Epple M, Schildhauer TA, Köller M (2014) Effect of silver nanoparticles on human mesenchymal stem cell differentiation. *Beilstein J Nanotechnol* **5**: 2058-2069.

Spriano S, Yamaguchi S, Bains F, Ferraris S (2018) A critical review of multifunctional titanium surfaces: new frontiers for improving osseointegration and host response, avoiding bacteria contamination. *Acta Biomater* **79**: 1-22.

Streitburger A, Henrichs MP, Hauschild G, Nottrott M, Guder W, Hardes J (2019) Silver-coated megaprotheses in the proximal femur in patients with sarcoma. *Eur J Orthop Surg Traumatol* **29**: 79-85.

Trujillo NA, Oldinski RA, Ma H, Bryers JD, Williams JD, Popat KC (2012) Antibacterial effects of silver-doped hydroxyapatite thin films sputter deposited on titanium. *Mater Sci Eng C* **32**: 2135-2144.

Wafa H, Grimer RJ, Reddy K, Jeys L, Abudu A, Carter SR, Tillman RM (2015) Retrospective evaluation of the incidence of early periprosthetic infection with silver-treated endoprostheses in high-risk patients: case-control study. *Bone Jt J* **97-B**: 252-257.

Wang W, Khoon C (2013) Titanium alloys in orthopaedics. In: *Titanium Alloys - Advances in Properties Control*. Editors: Sieniawski J and Ziaja W. DOI: 10.5772/55353.

Wojcieszak D, Mazur M, Kalisz M, Grobelny M (2017) Influence of Cu, Au and Ag on structural and surface properties of bioactive coatings based on titanium. *Mater Sci Eng C* **71**: 1115-1121.

Wyatt MC, Foxall-Smith M, Robertson A, Beswick A, Kieser DC, Whitehouse MR (2019) The use of silver

coating in hip megaprotheses: a systematic review. *Hip Int* **29**: 7-20.

Zhao L, Wang H, Huo K, Cui L, Zhang W, Ni H, Zhang Y, Wu Z, Chu PK (2011) Antibacterial nano-structured titania coating incorporated with silver nanoparticles. *Biomaterials* **32**: 5706-5716.

Web References

1. <https://imagej.net/Fiji> [31-05-2021]
2. <https://www.R-project.org/> [31-05-2021]

Discussion with Reviewer

Reviewer: Considering that the design goals for a Ag-loaded implant may not be entirely established, please comment on how the SN coating was designed to yield optimal performance in antibacterial and cell culture experiments.

Authors: Different coating techniques lead to different functionalities.

In the single Ag layer coating (SN), Ag ions were integrated into a thin Ti-nitride layer, providing a satisfactory antibacterial action with less compromise to osteoblast adhesion and proliferation than on the established dual-AG layer (SSN). Adjusting the molecular fraction of Ag in SN coatings might enabled cementless fixation of Ti implants that were protected from bacterial colonisation.

A coating with a base Ag layer lying under a superficial interrupted layer of AgTiN (SSN) led to a larger release of Ag ions and, thus, to slightly stronger antibacterial effects, but also to considerable toxicity to osteoblasts. SNN coatings could be useful for parts of the implant that are not in direct contact with bone.

Editor's note: The Scientific Editor responsible for this paper was Fintan Moriarty.